

Cite this: DOI: 00.0000/xxxxxxxxxx

# An exact expression of three-body system for the complex shear modulus of frictional granular materials

Michio Otsuki<sup>a</sup> and Hisao Hayakawa<sup>b</sup>Received Date  
Accepted Date

DOI: 00.0000/xxxxxxxxxx

We propose a simple model comprising three particles to study the nonlinear mechanical response of jammed frictional granular materials under oscillatory shear. Owing to the introduction of the simple model, we obtain an exact analytical expression of the complex shear modulus for a system including many monodispersed disks, which satisfies a scaling law in the vicinity of the jamming point. These expressions perfectly reproduce the shear modulus of the many-body system with low strain amplitudes and friction coefficients. Even for disordered many-body systems, the model reproduces results by introducing a single fitting parameter.

## 1 Introduction

The rheological property of densely dispersed grains, e.g., granular materials, colloidal suspensions, and emulsions, plays an important role in physics and engineering. This rheological property mainly depends on the packing fraction  $\phi$  of the grains. The materials behave like fluids for  $\phi < \phi_J$  with jamming fraction  $\phi_J$  and exhibit a solid-like elastic response above  $\phi_J$ <sup>1,2</sup>. In the linear response regime (i.e., for small strains), the shear modulus is characterized by the density of states<sup>3–5</sup> and satisfies scaling laws<sup>6–9</sup>. However, the linear response region becomes narrower as  $\phi$  approaches  $\phi_J$ <sup>10,11</sup>, and the nonlinear response becomes relevant due to the plastic deformation associated with the yielding<sup>12–20</sup>.

If we are interested in a nonlinear response to an applied oscillatory shear strain, it exhibits a complicated stress-strain curve. Although the storage and loss moduli  $G'$  and  $G''$  were originally introduced to characterize the linear viscoelasticity of materials, they can use to characterize nonlinear viscoelasticity or viscoelastoplastic responses to applied strains<sup>21</sup>. In this case,  $G'$  and  $G''$  are no longer constants but strongly depend on the strain amplitude  $\gamma_0$ . In particular, we have recognized that  $G'$  decreases with  $\gamma_0$ <sup>11,22–25</sup> and  $G''$  remains non-zero in the low frequency limit<sup>24,25</sup> for densely dispersed grains.

The theoretical analysis of densely dispersed grains is challenging as a typical many-body problem in non-equilibrium systems. To date, a few theoretical approaches have been proposed for systems related to frictionless particles. The scaling laws for the linear elastic response were derived in terms of the vibrational density of states<sup>7,8</sup>. The Fourier analysis of particle trajectories helps to generate semi-analytical expressions for  $G'$  and  $G''$ <sup>25</sup>. Unfortu-

nately, these theories can not apply to frictional particles because of the history-dependent contact force<sup>9,24</sup>.

It is helpful to analyze a simple model with small degrees of freedom to understand the behavior of many-body systems, including densely dispersed grains. This approach has been used in statistical mechanics. The mean-field approximation of the Ising model is a typical example in which the system contains only one Ising spin under the influence of a self-consistently determined mean field<sup>26</sup>. For atomic liquids, a cell model, in which a single atom exists in a cage, was used to derive the equation of state<sup>27,28</sup>. The coherent potential approximation for disordered solids has been used to understand electronic band structures<sup>29</sup>. The effective medium theory reveals the elastic response of random spring networks<sup>30</sup>. In addition, a simple model consisting of two particles was proposed to reproduce the liquid-solid phase transition<sup>31</sup>. The advantage of such few-body models is that we can obtain exact solutions. The qualitative behavior of the corresponding many-body systems can be determined based on the solutions of the few-body models. Thus, we adopt this approach to determine the nonlinear responses of the frictional dispersed grains.

This study proposes a model consisting of three identical particles to describe the mechanical response of jammed frictional granular materials under oscillatory shear. In Section 2, we introduce the three-body system (TBS). This model can be analytically solved for low-strain amplitudes and friction coefficients near the jamming point in Section 3. In Section 4, we demonstrate that the analytical solution reproduces the storage and loss moduli of many-body systems (MBSs) without any fitting parameter if there is no disorder in the particle configuration. Even if disorder exists, a scaling law for the complex shear modulus for the TBS semi-quantitatively agrees with the numerical simulations of the MBS by introducing a fitting parameter. We discuss and conclude our results in Section 5. In Appendix A, we show the details of the

<sup>a</sup> Graduate School of Engineering Science, Osaka University, Toyonaka, Osaka 560-8531, Japan. E-mail: m.otsuki.es@osaka-u.ac.jp

<sup>b</sup> Yukawa Institute for Theoretical Physics, Kyoto University, Kitashirakawa-iwake-cho, Sakyo-ku, Kyoto 606-8502, Japan.

MBS when the particles are initially placed on a triangular lattice. The effect of particle rotation is described in Appendix B. In Appendix C, we derive the analytical expressions for the shear stress and pressure in the TBS. In Appendix D, we relate the complex shear modulus with the hysteresis loop of the stress–strain curve. The details of the disordered MBS are presented in Appendix E. We present the numerical shear modulus for the TBS in Appendix F.

## 2 Three-Body System

We consider two-dimensional granular materials consisting of many grains under oscillatory shear (Fig. 1). Here, the grains constituting granular materials are modeled as frictional spherical particles. Moreover, we introduce a system of three identical particles to simply describe the MBS (Fig. 2). The MBS can contain polydisperse particles, while we assume that the TBS is a monodisperse system. In the TBS, the position  $\mathbf{r}_i(t) = (x_i(t), y_i(t))$  of particle  $i$  with diameter  $d$  at time  $t$  is given by

$$\mathbf{r}_1(t) = \left( \frac{\sqrt{3}\gamma(\theta(t))\ell}{4}, \frac{\sqrt{3}\ell}{4} \right), \quad (1)$$

$$\mathbf{r}_2(t) = \left( -\frac{\sqrt{3}\gamma(\theta(t))\ell}{4} - \frac{\ell}{2}, -\frac{\sqrt{3}\ell}{4} \right), \quad (2)$$

$$\mathbf{r}_3(t) = \left( -\frac{\sqrt{3}\gamma(\theta(t))\ell}{4} + \frac{\ell}{2}, -\frac{\sqrt{3}\ell}{4} \right), \quad (3)$$

where  $\ell$  is the initial distance between particles. We also introduce  $\varepsilon := 1 - \ell/d$  as the compressive strain. The compressive strain  $\varepsilon$  in the TBS corresponds to  $\phi - \phi_j$  in the MBS as shown in Appendix A. We apply shear strain as

$$\gamma(\theta) = \gamma_0 \sin \theta \quad (4)$$

with strain amplitude  $\gamma_0$ , phase  $\theta = \omega t$ , and angular frequency  $\omega$ . Note that we need at least three particles to realize a stable interlocking state.

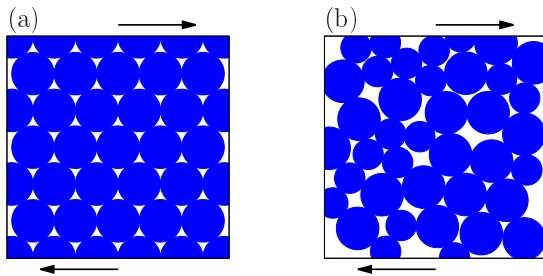


Fig. 1 Schematics of the ordered MBS (a) and the disordered MBS (b).

We adopt the interaction force  $\mathbf{f}_{ij}$  between particles  $i$  and  $j$  given by

$$\mathbf{f}_{ij} = \left( f_{ij}^{(n)} \mathbf{n}_{ij} + f_{ij}^{(t)} \mathbf{t}_{ij} \right) H(r_{ij} - d), \quad (5)$$

where  $f_{ij}^{(n)}$  and  $f_{ij}^{(t)}$  denote the normal and tangential forces between the particles  $i$  and  $j$ <sup>32</sup>. The distance between the particles  $i$  and  $j$  is  $r_{ij} = |\mathbf{r}_{ij}|$  with  $\mathbf{r}_{ij} := \mathbf{r}_i - \mathbf{r}_j = (x_{ij}, y_{ij})$ . Here,  $H(x)$  is

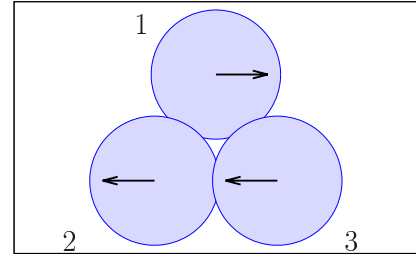


Fig. 2 A schematic of the TBS.

Heaviside's step function satisfying  $H(x) = 1$  for  $x > 0$  and  $H(x) = 0$  otherwise. The normal and tangential unit vectors are denoted by  $\mathbf{n}_{ij} := \mathbf{r}_{ij}/r_{ij} = (n_{ij,x}, n_{ij,y})$  and  $\mathbf{t}_{ij} := (-n_{ij,y}, n_{ij,x})$ , respectively. For simplicity, we do not consider the torque balance and, thus, the rotation of the particles. See Appendix B for the effect of the rotation.

The normal force is assumed to be

$$f_{ij}^{(n)} = -k_n u_{ij}^{(n)} \quad (6)$$

with the normal elastic constant  $k_n$  and normal relative displacement  $u_{ij}^{(n)} := r_{ij} - d$ . Moreover, the tangential force is assumed to be

$$f_{ij}^{(t)} = \min(|\tilde{f}_{ij}^{(t)}|, \mu f_{ij}^{(n)}) \text{sgn}(\tilde{f}_{ij}^{(t)}), \quad (7)$$

where  $\tilde{f}_{ij}^{(t)} = -k_t u_{ij}^{(t)}$ ;  $k_t$  denotes the tangential elastic constant, and  $\mu$  denotes the friction coefficient. Here,  $\min(a, b)$  selects the smaller value between  $a$  and  $b$ ,  $\text{sgn}(x) = 1$  for  $x \geq 0$ , and  $\text{sgn}(x) = -1$  for  $x < 0$ . The tangential displacement  $u_{ij}^{(t)}$  satisfies  $\frac{d}{dt} u_{ij}^{(t)} = v_{ij}^{(t)}$  for  $|\tilde{f}_{ij}^{(t)}| < \mu f_{ij}^{(n)}$  with the tangential velocity  $v_{ij}^{(t)} = (\frac{d}{dt} \mathbf{r}_i - \frac{d}{dt} \mathbf{r}_j) \cdot \mathbf{t}_{ij}$ , whereas  $u_{ij}^{(t)}$  remains unchanged for  $|\tilde{f}_{ij}^{(t)}| \geq \mu f_{ij}^{(n)}$ . We refer to the contact with  $|\tilde{f}_{ij}^{(t)}| < \mu f_{ij}^{(n)}$  as the stick contact and the contact with  $|\tilde{f}_{ij}^{(t)}| \geq \mu f_{ij}^{(n)}$  as the slip contact. The tangential displacement,  $u_{ij}^{(t)}$ , is initially set to zero.

The (symmetric contact) shear stress is given by

$$\sigma(\theta; \gamma_0, \mu) = \sigma^{(n)}(\theta; \gamma_0, \mu) + \sigma^{(t)}(\theta; \gamma_0, \mu) \quad (8)$$

with the normal component of  $\sigma$

$$\sigma^{(n)}(\theta; \gamma_0, \mu) = -\frac{1}{A} \sum_i \sum_{j>i} \frac{x_{ij} y_{ij}}{r_{ij}} f_{ij}^{(n)} \quad (9)$$

and tangential component of  $\sigma$

$$\sigma^{(t)}(\theta; \gamma_0, \mu) = -\frac{1}{2A} \sum_i \sum_{j>i} \frac{x_{ij}^2 - y_{ij}^2}{r_{ij}} f_{ij}^{(t)}. \quad (10)$$

Here,  $A$  corresponds to the area of the system, and we choose  $A = \sqrt{3}\ell^2/2$  as shown in Appendix A. The pressure is given by

$$P(\theta; \gamma_0, \mu) = \frac{1}{2A} \sum_i \sum_{j>i} (x_{ij} f_{ij,x} + y_{ij} f_{ij,y}). \quad (11)$$

In the right-hand sides of eqns. (9)-(11), we have omitted the arguments  $\theta$ ,  $\gamma_0$ , and  $\mu$ . Similar abbreviations are used below. As we are interested in quasistatic processes, we do not consider the

kinetic parts of  $\sigma$  and  $P$  and the dependence on  $\omega$ . After several cycles of oscillatory shear,  $\sigma(\theta)$  becomes periodic. The storage and loss moduli are given by<sup>33</sup>

$$G'(\gamma_0, \mu) = \frac{1}{\pi} \int_0^{2\pi} d\theta \sigma(\theta; \gamma_0, \mu) \sin \theta / \gamma_0, \quad (12)$$

$$G''(\gamma_0, \mu) = \frac{1}{\pi} \int_0^{2\pi} d\theta \sigma(\theta; \gamma_0, \mu) \cos \theta / \gamma_0. \quad (13)$$

### 3 Theoretical analysis

Assuming  $\gamma_0 \ll \varepsilon \ll 1$ , we analytically obtain  $G'$  and  $G''$  for the TBS. The derivation of the analytical results can be found in Appendix C.

First, the normal component of the shear stress is given by

$$\sigma^{(n)}(\theta) = \frac{\sqrt{3}k_n\gamma(\theta)}{4}. \quad (14)$$

The tangential component of the shear stress is given by

$$\sigma^{(t)}(\theta) = \frac{\sqrt{3}k_t\gamma(\theta)}{4} \quad (15)$$

for  $\gamma_0 < \gamma_c(\mu)$  with a critical amplitude

$$\gamma_c(\mu) = \frac{4\mu k_n \varepsilon}{3k_t}, \quad (16)$$

which characterizes the transition from stick to slip states in the contact between the particles. For  $\gamma_0 \geq \gamma_c(\mu)$ , the tangential component of the shear stress is given by

$$\sigma^{(t)}(\theta) = \begin{cases} \frac{\mu k_n \varepsilon}{\sqrt{3}}, & 0 \leq \theta < \frac{\pi}{2} \\ \frac{\mu k_n \varepsilon}{\sqrt{3}} + \frac{\sqrt{3}k_t(\gamma(\theta) - \gamma_0)}{4}, & \frac{\pi}{2} \leq \theta < \frac{\pi}{2} + \Theta \\ -\frac{\mu k_n \varepsilon}{\sqrt{3}}, & \frac{\pi}{2} + \Theta \leq \theta < \frac{3\pi}{2} \\ -\frac{\mu k_n \varepsilon}{\sqrt{3}} + \frac{\sqrt{3}k_t(\gamma(\theta) + \gamma_0)}{4}, & \frac{3\pi}{2} \leq \theta < \frac{3\pi}{2} + \Theta \\ \frac{\mu k_n \varepsilon}{\sqrt{3}}, & \frac{3\pi}{2} + \Theta \leq \theta < 2\pi, \end{cases} \quad (17)$$

where  $\Theta = \cos^{-1}(1 - 2\gamma_c(\mu)/\gamma_0)$ . Regions with  $\frac{\pi}{2} \leq \theta < \frac{\pi}{2} + \Theta$  and  $\frac{3\pi}{2} \leq \theta < \frac{3\pi}{2} + \Theta$  correspond to the stick state, and the other regions correspond to the slip state. Owing to this transition in the contact, the stress–strain curve given by eqns. (14)–(17) exhibits a hysteresis loop. Equation (17) does not exhibit a viscoelastic response but a typical elastoplastic response without viscous effect.

Figure 3 shows the scaled shear stress  $\sigma/\gamma_0$  against the scaled strain  $\gamma/\gamma_0$  using eqns. (4), (8), and (14)–(17) for various values of  $\gamma_0$  with  $k_t/k_n = 1.0$  and  $\mu = 0.01$ . The shape of the scaled stress–strain curve is characterized by a parallelogram as a typical elastoplastic response. As  $\gamma_0$  increases, the maximum value  $\bar{\sigma}_{\max} = (\sigma/\gamma_0)|_{\gamma/\gamma_0=1}$  decreases from a larger value  $\sqrt{3}(k_n + k_t)/4$  to a smaller value  $\sqrt{3}k_n/4$ . As shown in Appendix D, the storage modulus  $G'$  is approximately given by  $\bar{\sigma}_{\max}$ . Hence, the decrease of  $\bar{\sigma}_{\max}$  in Fig. 3 indicates the decrease of  $G'$ . For  $\gamma_0 = 0.00003$  and 0.0001, the hysteresis loop exists, but the area of the loop is negligible for  $\gamma_0 = 0.00001$  and 0.001. The loss modulus  $G''$  is pro-

portional to the area of the loop as shown in Appendix D. Hence, the dependence of the area on  $\gamma_0$  indicates that there is a peak in  $G''$  as  $\gamma_0$  increases.

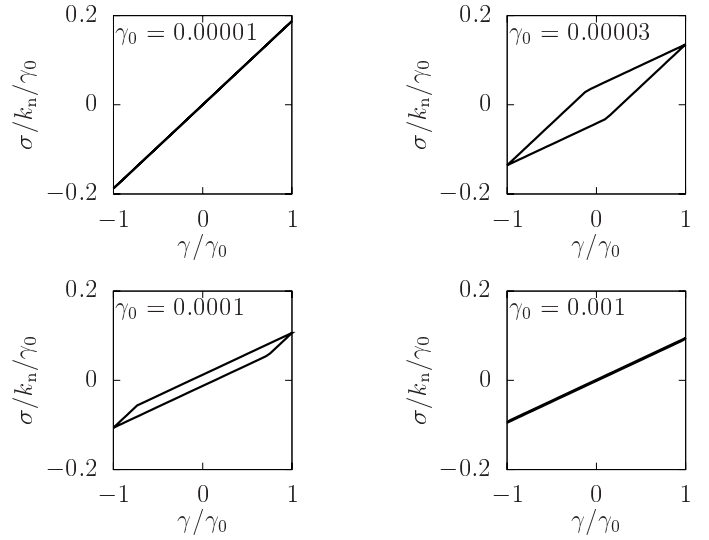


**Fig. 3** Scaled shear stress  $\sigma/\gamma_0$  against  $\gamma/\gamma_0$  using eqns. (4), (8), and (14)–(17) for various values of  $\gamma_0$  with  $k_t/k_n = 1.0$ ,  $\varepsilon = 0.001$ , and  $\mu = 0.01$ .

Substituting eqns. (8) and (14)–(17) into eqn. (12), we obtain the storage modulus as

$$G' = \begin{cases} \frac{\sqrt{3}(k_n + k_t)}{4}, & \gamma_0 \leq \gamma_c(\mu) \\ \frac{\sqrt{3}}{4} \left\{ k_n + \frac{k_t}{\pi} (\Theta - \sin \Theta \cos \Theta) \right\}, & \gamma_0 > \gamma_c(\mu). \end{cases} \quad (18)$$

As  $\gamma_0$  increases beyond  $\gamma_c(\mu)$ ,  $G'$  decreases from a higher value to a lower value. The corresponding behavior has been observed in the MBS in previous studies<sup>9,24</sup>.

Substituting eqns. (8) and (14)–(17) into eqn. (13), the loss modulus is given by

$$G'' = \begin{cases} 0, & \gamma_0 \leq \gamma_c(\mu) \\ \frac{\sqrt{3}k_t}{4\pi} (1 - \cos^2 \Theta), & \gamma_0 > \gamma_c(\mu). \end{cases} \quad (19)$$

The loss modulus  $G''$  is zero for  $\gamma_0 < \gamma_c(\mu)$ , whereas  $G''$  sharply increases with  $\gamma_0$  when  $\gamma_0$  exceeds  $\gamma_c(\mu)$  and decreases to 0 after a peak. The behavior of  $G''$  for the TBS qualitatively reproduces that of the MBS in previous studies<sup>24</sup>.

We adopt the abbreviation for the pressure at  $\gamma = 0$  as

$$P_0 := P(\theta = 0; \gamma_0, \mu), \quad (20)$$

which is also obtained as

$$P_0 = \sqrt{3}k_n \varepsilon. \quad (21)$$

From eqns. (16), (18), (19), and (21), we derive scaling laws for

a given  $\varepsilon$  as

$$G'(\mu, \gamma_0) = G'_M(\mu) \mathcal{G}'\left(\frac{k_t \gamma_0}{\mu P_0(\gamma_0, \mu)}\right), \quad (22)$$

$$G''(\mu, \gamma_0) = G''_M(\mu) \mathcal{G}''\left(\frac{k_t \gamma_0}{\mu P_0(\gamma_0, \mu)}\right), \quad (23)$$

where  $\mathcal{G}'(x)$  and  $\mathcal{G}''(x)$  denote scaling functions. The maximum values of  $G'$  and  $G''$  are denoted as  $G'_M$  and  $G''_M$ , respectively. In the TBS, they are given as

$$G'_M = \sqrt{3}(k_n + k_t)/4, \quad G''_M = \sqrt{3}k_t/(4\pi), \quad (24)$$

$$\mathcal{G}'(x) = \begin{cases} 1, & x \leq x_c, \\ \left(1 + \frac{k_t}{k_n} \frac{T(x) - S(x)}{\pi}\right) / \left(1 + \frac{k_t}{k_n}\right), & x > x_c, \end{cases} \quad (25)$$

$$\mathcal{G}''(x) = \begin{cases} 0, & x \leq x_c, \\ 1 - \cos^2 T(x), & x > x_c \end{cases} \quad (26)$$

with  $T(x) = \cos^{-1}(1 - 2x_c/x)$ ,  $S(x) = \sin(2T(x))/2$ , and  $x_c = 4/(3\sqrt{3})$ .

## 4 Comparison with the MBS

We demonstrate the relevance of the TBS analysis based on the simulation of a two-dimensional MBS consisting of  $N$  frictional grains. First, we consider a system corresponding to the TBS, where all the particles are identical and initially placed on the triangular lattice with a unit length  $\ell$  (Fig. 1(a)). The details are shown in Appendix A. Next, we consider a bidisperse system where the number of particles with diameter  $d$  is equal to that of particles with diameter  $d/1.4$ , and the particles are randomly placed with packing fraction  $\phi$  (Fig. 1(b)). The mass densities of the particles are identical. The details of the disordered MBS are shown in Appendix E. In both systems, the shear strain given by eqn. (4) is applied for  $N_c$  cycles using the SLLOD equation under the Lees–Edwards boundary condition<sup>34</sup>. In the MBS, we replace the normal force as

$$f_{ij}^{(n)} \rightarrow -\left(k_n u_{ij}^{(n)} + \eta_n v_{ij}^{(n)}\right) \quad (27)$$

with the normal viscous constant  $\eta_n$  and the normal velocity  $v_{ij}^{(n)} = \left(\frac{d}{dt} \mathbf{r}_i - \frac{d}{dt} \mathbf{r}_j\right) \cdot \mathbf{n}_{ij}$  to include the viscous force depending on the relative velocity. The tangential force is replaced by

$$f_{ij}^{(t)} \rightarrow \min\left(|\tilde{f}_{ij}^{(t)}|, \mu f_{ij}^{(n,el)}\right) \text{sgn}(\tilde{f}_{ij}^{(t)}), \quad (28)$$

with

$$\tilde{f}_{ij}^{(t)} \rightarrow -\left(k_t u_{ij}^{(t)} + \eta_t v_{ij}^{(t)}\right), \quad (29)$$

where  $f_{ij}^{(n,el)} = -k_n u_{ij}^{(n)}$  denotes the elastic part of the normal force with a tangential viscous constant  $\eta_t$ . We measure  $G'$ ,  $G''$ , and  $P_0$  in the last cycle using eqns. (11)-(13). For the ordered MBS, we use  $N = 64$ ,  $k_t/k_n = 1.0$ , and  $\varepsilon = 0.001$ , whereas  $N = 1000$ ,  $k_t/k_n = 0.2$ , and  $\phi = 0.87$  are used for the disordered MBS. In both systems, the other parameters are identical:  $N_c = 20$ ,  $\eta_t = \eta_n = \sqrt{m k_n}$ , and  $\omega = 0.0001 \sqrt{m/k_n}$  with a mass  $m$  of larger particles.

As shown in Fig. 4, we plot  $G'$  for the ordered MBS against  $\gamma_0$

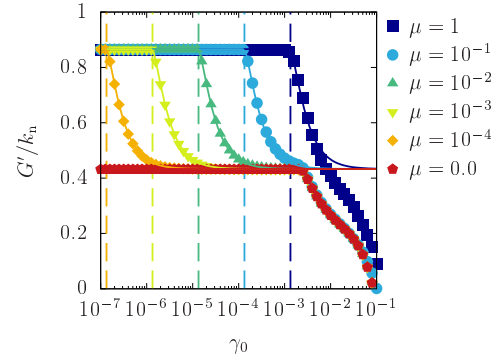


**Fig. 4** Storage modulus  $G'$  against  $\gamma_0$  with  $k_t/k_n = 1.0$  and  $\varepsilon = 0.001$  for various values of  $\mu$ . The points represent the results of the ordered MBS. The thin solid lines represent the analytical result given by eqn. (18). The vertical dashed lines represent the critical amplitude  $\gamma_c(\mu)$  given by eqn. (16) for  $\mu = 10^{-4}, 10^{-3}, 10^{-2}, 10^{-1}$ , and 1 from left to right.

with  $k_t/k_n = 1.0$  and  $\varepsilon = 0.001$  for various values of  $\mu$  as points. Moreover, we plot the analytical results of the TBS obtained using eqn. (18) as thin solid lines. Surprisingly, the results of the TBS agree with those of the MBS for  $\gamma_0 < 0.003$  without any fitting parameters. As  $\gamma_0$  increases beyond  $\gamma_c(\mu)$  shown by the vertical dashed lines,  $G'$  for  $\mu > 0$  decreases and converges to a constant, which is equal to  $G'$  for  $\mu = 0$ . For larger  $\gamma_0$ ,  $G'$  for the MBS decreases again, whereas the theoretical  $G'$  for the TBS is constant. This discrepancy results from the violation of condition  $\gamma_0 \ll \varepsilon$  for the analytical calculation. If we numerically solve the TBS to obtain  $G'$  without the assumption  $\gamma_0 \ll \varepsilon$ ,  $G'$  decreases after a plateau again as in the case of MBS, although its value in the TBS for  $\gamma_0 \rightarrow 0.1$  slightly deviates from that of the MBS, as shown in Appendix F.

As shown in Fig. 5, we plot  $G''$  for the MBS on the triangular lattice against  $\gamma_0$  with  $k_t/k_n = 1.0$  and  $\varepsilon = 0.001$  for various values of  $\mu$  as points. Moreover, we plot the analytical results of the TBS obtained using eqn. (19) as thin solid lines. The analytical result agrees perfectly with the MBS for  $\gamma_0 < 0.003$  without any fitting parameters. As  $\gamma_0$  increases beyond  $\gamma_c(\mu)$  shown by the vertical dashed lines,  $G''$  for  $\mu > 0$  increases from 0 and decreases after reaching a peak. The peak position of  $G''$  against  $\gamma_0$  increases with  $\mu$ . Thus, our analytical results fail to capture the behavior of  $G''$  for  $\mu = 1$ .

Consider the disordered MBS shown in Fig. 1(b). Figure 6 shows the scaled shear stress  $\sigma/\gamma_0$  against the scaled strain  $\gamma/\gamma_0$  in the disordered MBS with  $\mu = 0.0001$ . The maximum value  $\tilde{\sigma}_{\max}$  decreases as  $\gamma_0$  increases. The area  $S$  of the curve is the largest for  $\gamma_0 = 0.00003$ . It is interesting that stress-strain curves are not characterized by parallelograms in this case in contrast to Fig. 3. This means that the disordered configuration of particles creates an effective viscosity, and thus, the response to an applied strain becomes visco-elastoplastic.

The behaviors of  $G'$  and  $G''$  in the disordered MBS are similar to those of the TBS as shown in Appendix E. Therefore, it is expected that the scaling laws in eqns. (22) and (23) for a given  $\varepsilon$  in the TBS can be used even in this system with corresponding  $\phi$ . This expectation is verified by Fig. 7, in which we plot the scaled mod-

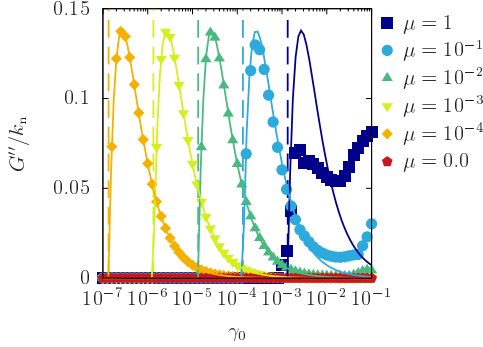


**Fig. 5** Loss modulus  $G''$  against  $\gamma_0$  with  $k_t/k_n = 1.0$  and  $\varepsilon = 0.001$  for various values of  $\mu$ . The points represent the results of the ordered MBS. The thin solid lines represent the analytical results obtained using eqn. (19). The vertical dashed lines represent the critical amplitude  $\gamma_c(\mu)$  given by eqn. (16) for  $\mu = 10^{-4}, 10^{-3}, 10^{-2}, 10^{-1}$ , and 1 from left to right.

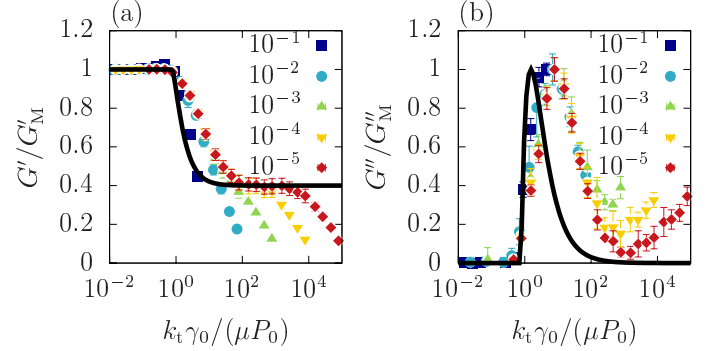


**Fig. 7** (a) Scaled storage modulus  $G'/G'_M$  against the scaled strain  $k_t\gamma_0/(\mu P_0(\gamma_0, \mu))$  with  $\phi = 0.87$  and  $k_t/k_n = 0.2$  for various values of  $\mu$  in the disordered MBS. The solid line represents the analytical result of the TBS given by eqn. (25) with  $k_t/k_n = 1.5$ . (b) Scaled loss modulus  $G''/G''_M$  against the scaled strain  $k_t\gamma_0/(\mu P_0(\gamma_0, \mu))$  with  $\phi = 0.87$  and  $k_t/k_n = 0.2$  for various values of  $\mu$  in the disordered MBS. The solid line represents the analytical result of the TBS given by eqn. (26) with  $k_t/k_n = 1.5$ .

## 5 Conclusions

We demonstrated the relevancy of a model of the TBS to describe the complex modulus of jammed frictional granular materials under oscillatory shear. We obtained the analytical expressions for the  $\gamma_0$ -dependence of  $G'$  and  $G''$  as shown in eqns. (16), (18), and (19), which predict the  $\mu$ -dependence of the critical amplitude  $\gamma_c$ , the decrease of  $G'$ , and the peak of  $G''$  above  $\gamma_c$  for crystalline solids. The analytical expressions lead to the scaling laws given by eqns. (22) and (23). Although we have ignored the non-affine motion for crystalline solids, these analytical results quantitatively agree with those of the ordered MBS. Surprisingly, some characteristic features of disordered solids for low strain (or high pressure) can be captured. These results indicate that the analysis of the toy model gives a basis for understanding the nonlinear rheology of frictional granular materials under small strain.

Although the values of the plateaus in  $G'$  for disordered MBS depended on  $\phi - \phi_J^{6,9}$ , the corresponding values of the TBS are independent of  $\phi - \phi_J$ , as expressed in eqn. (18). In addition, our analytical expressions cannot reproduce the second decrease of  $G'$  and increase of  $G''$  near  $\gamma_0 = 10^{-2}$  in the MBS. The discrepancy should result from the disorder because it leads to the  $\phi$ -dependence of  $G'$ . To include the disorder effect, we regarded  $k_t/k_n$  as a fitting parameter. In previous studies on models with small degrees of freedom, e.g., the coherent potential approximation<sup>26,29,30</sup>, the corresponding fitting parameters were self-consistently determined. In future studies, we will discuss the self-consistent determination of the parameter for the TBS.

Some researchers are interested in contributions from higher

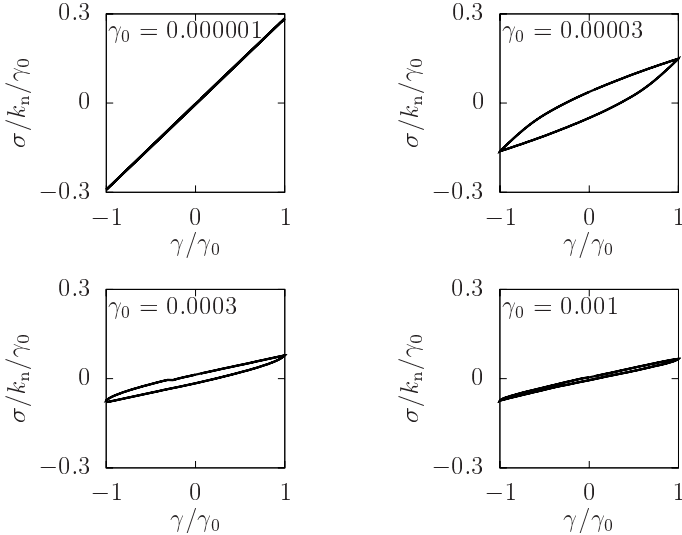


**Fig. 6** Scaled shear stress  $\sigma/\gamma_0$  against  $\gamma/\gamma_0$  in the disordered MBS for various values of  $\gamma_0$  with  $\mu = 0.01$  and  $\phi = 0.870$ .

harmonics characterizing the nonlinear response to oscillatory shear<sup>21</sup>, but the nonlinear viscoelastic moduli characterizing the higher harmonics are negligibly small for jammed frictionless particles<sup>25</sup>. However, the higher harmonics in the frictional granular materials require further careful investigation.

## Conflicts of interest

There are no conflicts to declare.

## Appendix A: Details of Ordered MBS

This section explains the details of the ordered MBS consisting of monodispersed particles initially placed on a triangular lattice. We consider a two-dimensional assembly of  $N$  frictional particles in a periodic box with sizes along the  $x$  and  $y$  directions  $L_x$  and  $L_y$ , respectively. Here, we initially place  $N = 2N_x N_y$  particles of diameter  $d$  with integers  $n_x$  and  $n_y$  at  $\mathbf{r}_i$  as

$$\mathbf{r}_i = \left( n_x \ell - L_x/2, \sqrt{3} n_y \ell - L_y/2 \right) \quad (30)$$

for  $0 \leq i < N_x N_y$  with integers  $n_x, n_y$ , and  $i = n_x + N_x n_y$ . For  $N_x N_y \leq i < 2N_x N_y$ ,  $\mathbf{r}_i$  is defined as

$$\mathbf{r}_i = \left( (n_x + 1/2)\ell - L_x/2, \sqrt{3}(n_y + 1/2)\ell - L_y/2 \right) \quad (31)$$

with  $i = n_x + N_x n_y + N_x N_y$ . The initial configuration is illustrated in Fig. 8. We choose  $L_x = N_x \ell$  and  $L_y = \sqrt{3} N_y \ell$  with  $\ell = d(1 - \varepsilon)$ .

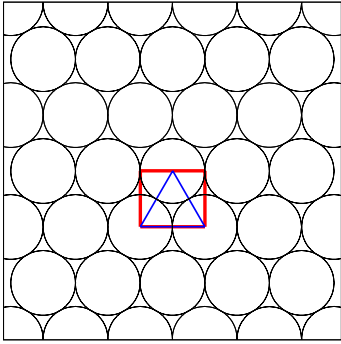


**Fig. 8** Initial configuration of mono-dispersed particles on a triangular lattice. The red rectangle, including interactions represented by the blue lines, corresponds to the TBS.

The position  $\mathbf{r}_i$  and peculiar momentum  $\mathbf{p}_i$  of particle  $i$  with mass  $m_i$  and diameter  $d_i$  are driven by the SLLOD equation under the Lees-Edwards boundary condition as<sup>34</sup>

$$\frac{d}{dt} \mathbf{r}_i = \dot{\gamma}(t) y_i \mathbf{e}_x + \frac{\mathbf{p}_i}{m_i}, \quad (32)$$

$$\frac{d}{dt} \mathbf{p}_i = -\dot{\gamma}(t) p_{i,y} \mathbf{e}_x + \mathbf{f}_i, \quad (33)$$

where  $\dot{\gamma}(t) = \gamma_0 \omega \cos \omega t$  and  $\mathbf{e}_x = (1, 0)$  is the unit vector along the  $x$  direction. The interaction force  $\mathbf{f}_i$  is defined as

$$\mathbf{f}_i = \sum_{j \neq i} \left( f_{ij}^{(n)} \mathbf{n}_{ij} + f_{ij}^{(t)} \mathbf{t}_{ij} \right) H(d_{ij} - r_{ij}) \quad (34)$$

with  $d_{ij} = (d_i + d_j)/2$ ,  $\mathbf{n}_{ij} = \mathbf{r}_{ij}/r_{ij}$ ,  $\mathbf{t}_{ij} = (-n_{ij,y}, n_{ij,x})$ , and  $\mathbf{r}_{ij} =$

$\mathbf{r}_i - \mathbf{r}_j = (x_{ij}, y_{ij})$ . The normal force is given by

$$f_{ij}^{(n)} = - \left( k_n u_{ij}^{(n)} + \eta_n v_{ij}^{(n)} \right) \quad (35)$$

with a normal viscous constant  $\eta_n$  and

$$v_{ij}^{(n)} = (\mathbf{v}_i - \mathbf{v}_j) \cdot \mathbf{n}_{ij}, \quad (36)$$

where the velocity of particle  $i$  is given by  $\mathbf{v}_i = \frac{d}{dt} \mathbf{r}_i$ . The following model is adopted for the tangential force:

$$f_{ij}^{(t)} = \min \left( |\tilde{f}_{ij}^{(t)}|, \mu f_{ij}^{(n,el)} \right) \text{sgn}(\tilde{f}_{ij}^{(t)}), \quad (37)$$

where  $f_{ij}^{(n,el)} = -k_n u_{ij}^{(n)}$  denotes the elastic part of the normal force. Here,  $\tilde{f}_{ij}^{(t)}$  is given by

$$\tilde{f}_{ij}^{(t)} = - \left( k_t u_{ij}^{(t)} + \eta_t v_{ij}^{(t)} \right) \quad (38)$$

with a tangential viscous constant  $\eta_t$ . The tangential velocity  $v_{ij}^{(t)}$  is given by

$$v_{ij}^{(t)} = (\mathbf{v}_i - \mathbf{v}_j) \cdot \mathbf{t}_{ij}. \quad (39)$$

The tangential displacement  $u_{ij}^{(t)}$  satisfies  $\frac{d}{dt} u_{ij}^{(t)} = v_{ij}^{(t)}$  for  $|\tilde{f}_{ij}^{(t)}| < \mu f_{ij}^{(n,el)}$ , whereas  $u_{ij}^{(t)}$  remains unchanged for  $|\tilde{f}_{ij}^{(t)}| \geq \mu f_{ij}^{(n,el)}$ . The tangential displacement  $u_{ij}^{(t)}$  is set to zero if  $i$  and  $j$  are detached.

If all the particles are separated, the packing fraction  $\phi$  for the ordered MBS is defined as

$$\phi = \frac{\sum_i \pi d_i^2}{4L_x L_y}. \quad (40)$$

Even if contacts exist between the particles, we use eqn. (40) by assuming that the contact length  $d_{ij} - r_{ij}$  is sufficiently lower than  $d_{ij}$ . Using eqn. (40),  $\phi$  is defined as

$$\phi = \frac{\pi}{2\sqrt{3}(1 - \varepsilon)^2}. \quad (41)$$

The jamming point of this system is

$$\phi_1 = \frac{\pi}{2\sqrt{3}} \quad (42)$$

with  $\varepsilon = 0$ . The distance from the jamming point is proportional to  $\varepsilon$ .

$$\phi - \phi_1 \simeq \frac{\pi}{\sqrt{3}} \varepsilon \quad (43)$$

for  $\varepsilon \ll 1$ .

The shear stress  $\sigma$  is defined by eqn. (8) in the main article with the normal component

$$\sigma^{(n)} = - \frac{1}{L_x L_y} \sum_i \sum_{j>i} \frac{x_{ij} y_{ij}}{r_{ij}} f_{ij}^{(n)} \quad (44)$$

and tangential component

$$\sigma^{(t)} = - \frac{1}{2L_x L_y} \sum_i \sum_{j>i} \frac{x_{ij}^2 - y_{ij}^2}{r_{ij}} f_{ij}^{(t)}. \quad (45)$$

The pressure is defined as

$$P = \frac{1}{2L_x L_y} \sum_i \sum_{j>i} (x_{ij} f_{ij,x} + y_{ij} f_{ij,y}). \quad (46)$$

We use  $N_x = 8$ ,  $N_y = 4$ ,  $N_c = 20$ ,  $k_t = k_n$ , and  $\eta_n = \eta_t = k_n \sqrt{m/k_n}$ , where  $m$  denotes the mass of a particle with diameter  $d$ . This model corresponds to a restitution coefficient  $e = 0.043$ . We adopt the leapfrog algorithm considering a time step of  $\Delta t = 0.05t_0$ . We choose  $\omega = 1.0 \times 10^{-4} \sqrt{k_n/m}$  as the quasistatic shear deformation because  $G'$  and  $G''$  are almost independent of  $\omega$  for  $\omega \leq 1.0 \times 10^{-3} \sqrt{k_n/m}$ .

As shown in Figs. 4 and 5, the behaviors of  $G'$  and  $G''$  of the TBS agree with that of the MBS. We explain the theoretical background of the TBS. The initial configuration is shown in Fig. 8; it contains the unit cell represented by the red rectangle with length  $\ell$  and height  $\sqrt{3}\ell/2$ . It contains interactions between the three particles represented by blue lines. Here, we assume that the particles move affinely as

$$\mathbf{r}_i(t) = \mathbf{r}_i(0) + \gamma(\theta(t))y_i(0)\mathbf{e}_x. \quad (47)$$

In this case, the corresponding relative distances between the particles in any unit cell are identical.

In particular, in a unit cell containing particles  $i = i_1, i_2$ , and  $i_3$  with  $i_1 = N_x N_y$ ,  $i_2 = 0$ , and  $i_3 = 1$ , the positions of the particles are given by

$$\mathbf{r}_{i_1}(t) = \left( \gamma(\theta(t)) \left( \frac{\sqrt{3}\ell - L_y}{2} \right) + \frac{\ell - L_x}{2}, \frac{\sqrt{3}\ell - L_y}{2} \right), \quad (48)$$

$$\mathbf{r}_{i_2}(t) = \left( -\gamma(\theta(t)) \frac{L_y}{2} - \frac{L_x}{2}, -\frac{L_y}{2} \right), \quad (49)$$

$$\mathbf{r}_{i_3}(t) = \left( -\gamma(\theta(t)) \frac{L_y}{2} + \ell - \frac{L_x}{2}, -\frac{L_y}{2} \right). \quad (50)$$

The relative distances between these particles are identical to those of the TBS, given by eqns. (1)-(3), which indicates that the TBS provides the interaction forces among the three particles. This system includes  $2N_x N_y$  unit cells with identical interaction forces. Hence, the normal and tangential components of  $\sigma$  are given by

$$\sigma^{(n)} = -\frac{2N_x N_y}{L_x L_y} \sum_{i=i_1, i_2, i_3} \left\{ \sum_{\substack{j=i_1, i_2, i_3 \\ (j>i)}} \frac{x_{ij} y_{ij}}{r_{ij}} f_{ij}^{(n)} \right\}, \quad (51)$$

$$\sigma^{(t)} = -\frac{N_x N_y}{L_x L_y} \sum_{i=i_1, i_2, i_3} \left\{ \sum_{\substack{j=i_1, i_2, i_3 \\ (j>i)}} \frac{x_{ij}^2 - y_{ij}^2}{r_{ij}} f_{ij}^{(t)} \right\}. \quad (52)$$

The pressure is also given by:

$$P = \frac{N_x N_y}{L_x L_y} \sum_{i=i_1, i_2, i_3} \left\{ \sum_{\substack{j=i_1, i_2, i_3 \\ (j>i)}} (x_{ij} f_{ij,x} + y_{ij} f_{ij,y}) \right\}. \quad (53)$$

Using the relation  $L_x L_y / (2N_x N_y) = \sqrt{3}\ell^2/2$  corresponding to  $A = \sqrt{3}\ell^2/2$ ,  $\sigma^{(n)}$ ,  $\sigma^{(t)}$ , and  $P$  coincide with eqns. (8)-(11). Hence, if the assumptions of the affine motion, i.e., eqns. (48)-(50), are satisfied,  $G'$  and  $G''$  in the ordered MBS coincide with those in the TBS.

## Appendix B: Effect of particle rotation

In this section, we illustrate the effect of particle rotation, which was not described in Appendix A. In the model with rotation, the tangential velocity  $v_{ij}^{(t)}$  is given by

$$v_{ij}^{(t)} = (\mathbf{v}_i - \mathbf{v}_j) \cdot \mathbf{t}_{ij} - (d_i \omega_i + d_j \omega_j)/2 \quad (54)$$

instead of eqn. (39), where  $\omega_i$  denotes the angular velocity of particle  $i$ . The time evolution of  $\omega_i$  is given by

$$I_i \frac{d}{dt} \omega_i = T_i \quad (55)$$

with the moment of inertia  $I_i = m_i d_i^2/8$  and torque  $T_i = -\sum_j \frac{d_i}{2} \mathbf{F}_{ij}^{(t)} \cdot \mathbf{t}_{ij}$ .

As shown in Fig. 9, we plot  $G'$  in the ordered MBS with and without rotation with  $k_t/k_n = 1.0$  and  $\varepsilon = 0.001$  for various values of  $\mu = 0.01$ . The values of other parameters are the same as those in Appendix A. The effect of particle rotation is negligible, except for the region near  $\gamma_c$ .

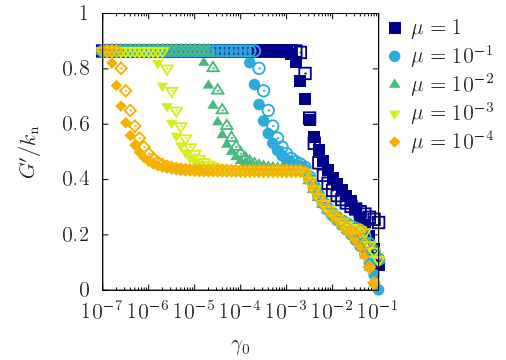


**Fig. 9** Storage modulus  $G'$  against  $\gamma_0$  for the ordered MBS with  $\mu = 0.01$  and  $\varepsilon = 0.001$ . The open and filled symbols represent the results of the particles with and without rotation, respectively.

As shown in Fig. 10, we plot  $G''$  in the ordered MBS with and without rotation with  $k_t/k_n = 1.0$  and  $\varepsilon = 0.001$  for  $\mu = 10^{-2}, 10^{-3}, 10^{-4}, 10^{-5}$  and  $0.00001$ . The values of other parameters are the same as those in Appendix A. There are slight deviations in the peak position near  $\gamma_c$  between particles with and without rotation.

In Fig. 11, we plot  $G''$  in the ordered MBS with and without rotation with  $k_t/k_n = 1.0$  and  $\varepsilon = 0.001$  for  $\mu = 1.0$  and  $0.1$ . There are slight deviations in the peak position near  $\gamma_c$  between particles with and without rotation even for these higher  $\mu$ . In addition, the second increase in  $G''$  around  $\gamma_0 = 0.1$  for particles without rotation disappears for those with rotation.

## Appendix C: Analytical calculation of shear stress and pressure

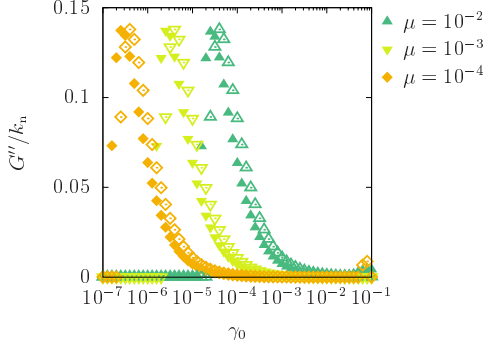


**Fig. 10** Loss modulus  $G''$  against  $\gamma_0$  for the ordered MBS with  $\mu = 10^{-2}, 10^{-3}, 10^{-4}, 10^{-5}$  and  $\varepsilon = 0.001$ . The open and filled symbols represent the results of the particles with and without rotation, respectively.

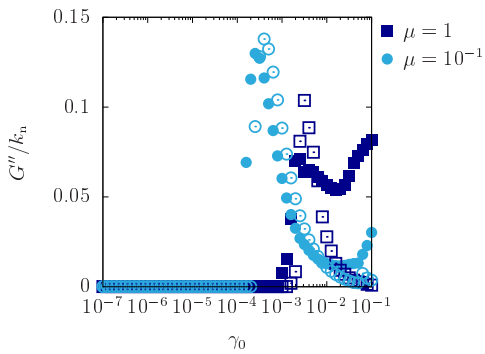


**Fig. 11** Loss modulus  $G''$  against  $\gamma_0$  for the ordered MBS with  $\mu = 1.0, 0.1$  and  $\varepsilon = 0.001$ . The open and filled symbols represent the results of the particles with and without rotation, respectively.

This section briefly explains the derivation of the normal and tangential components of shear stress and pressure for a small value of  $\gamma_0$ . From eqns. (1)–(3), the relative distance  $\mathbf{r}_{ij}(t)$  is given by

$$\mathbf{r}_{12}(\theta(t)) = \left( \frac{\sqrt{3}\gamma(\theta(t)) + 1}{2}\ell, \frac{\sqrt{3}\ell}{2} \right), \quad (56)$$

$$\mathbf{r}_{13}(\theta(t)) = \left( \frac{\sqrt{3}\gamma(\theta(t)) - 1}{2}\ell, \frac{\sqrt{3}\ell}{2} \right), \quad (57)$$

$$\mathbf{r}_{23}(\theta(t)) = (-\ell, 0). \quad (58)$$

Substituting these equations into  $u_{ij}^{(n)} = r_{ij} - d$ , the normal displacements are given by

$$u_{12}^{(n)}(t) = -\varepsilon d + \frac{\sqrt{3}}{4}\ell\gamma(\theta(t)) + O(\gamma_0^2), \quad (59)$$

$$u_{13}^{(n)}(t) = -\varepsilon d - \frac{\sqrt{3}}{4}\ell\gamma(\theta(t)) + O(\gamma_0^2), \quad (60)$$

$$u_{23}^{(n)}(t) = -\varepsilon d. \quad (61)$$

Substituting these equations into eqn. (6), we obtain the normal force as

$$f_{12}^{(n)} = k_n \left( \varepsilon d - \frac{\sqrt{3}}{4}\gamma(\theta)\ell \right), \quad (62)$$

$$f_{13}^{(n)} = k_n \left( \varepsilon d - \frac{\sqrt{3}}{4}\gamma(\theta)\ell \right), \quad (63)$$

$$f_{23}^{(n)} = k_n \varepsilon d \quad (64)$$

up to  $O(\gamma_0)$ .

By differentiating eqns. (56)–(58) with time  $t$ , we obtain the relative velocity as

$$\mathbf{v}_{12}(t) = \left( \frac{\sqrt{3}\dot{\gamma}(\theta(t))\ell}{2}, 0 \right), \quad (65)$$

$$\mathbf{v}_{13}(t) = \left( \frac{\sqrt{3}\dot{\gamma}(\theta(t))\ell}{2}, 0 \right), \quad (66)$$

$$\mathbf{v}_{23}(t) = (0, 0) \quad (67)$$

with the strain rate  $\dot{\gamma}(\theta(t)) = \frac{d}{dt}\gamma(\theta(t))$ . The tangential unit vector



is given by

$$\mathbf{t}_{12}(t) = \left( -\frac{\sqrt{3}\ell}{2}, \frac{\sqrt{3}\gamma(\theta(t))+1}{2}\ell \right) / |\mathbf{r}_{12}|, \quad (68)$$

$$\mathbf{t}_{13}(t) = \left( -\frac{\sqrt{3}\ell}{2}, \frac{\sqrt{3}\gamma(\theta(t))-1}{2}\ell \right) / |\mathbf{r}_{13}|, \quad (69)$$

$$\mathbf{t}_{23}(t) = (0, -1). \quad (70)$$

By considering the inner product of  $\mathbf{v}_{ij}$  and  $\mathbf{t}_{ij}$ , the tangential velocity is given by

$$v_{12}^{(t)}(t) = -\frac{3}{4}\ell\dot{\gamma}(\theta(t)) + O(\gamma_0^2), \quad (71)$$

$$v_{13}^{(t)}(t) = -\frac{3}{4}\ell\dot{\gamma}(\theta(t)) + O(\gamma_0^2), \quad (72)$$

$$v_{23}^{(t)}(t) = 0. \quad (73)$$

If the transition from the stick state to the slip state does not occur under oscillatory shear, the tangential displacement is obtained by integrating  $v_{ij}^{(t)}(t)$  as

$$u_{12}^{(t)}(t) = u_{13}^{(t)}(t) = -\frac{3}{4}\ell\gamma(\theta(t)) + O(\gamma_0^2), \quad (74)$$

$$u_{23}^{(t)}(t) = 0. \quad (75)$$

Substituting these equations into  $f_{ij}^{(t)} = -k_t u_{ij}^{(t)}$  yields

$$f_{12}^{(t)} = f_{13}^{(t)} = 3k_t\gamma(\theta(t))\ell/4, \quad (76)$$

$$f_{23}^{(t)} = 0 \quad (77)$$

up to  $O(\gamma_0)$ . The condition that the transition does not occur is satisfied when  $f_{12}^{(t)} < \mu f_{12}^{(n)}$  for  $\gamma = \gamma_0$ . Using eqns. (62) and (76) with the assumption  $\gamma_0 \ll \varepsilon$ , the condition is replaced by  $\gamma_0 < \gamma_c$  with  $\gamma_c$  given by eqn. (16).

For  $\gamma_0 > \gamma_c$ , there exist regions where  $u_{ij}^{(t)}$  is unchanged in the slip state as

$$u_{12}^{(t)} = \begin{cases} -\frac{\mu k_n \varepsilon d}{k_t}, & 0 \leq \theta(\theta) < \frac{\pi}{2} \\ -\frac{\mu k_n \varepsilon d}{k_t} - \frac{3d(\gamma(\theta) - \gamma_0)}{4}, & \frac{\pi}{2} \leq \theta < \frac{\pi}{2} + \Theta \\ \frac{\mu k_n \varepsilon d}{k_t}, & \frac{\pi}{2} + \Theta \leq \theta < \frac{3\pi}{2} \\ \frac{\mu k_n \varepsilon d}{k_t} - \frac{3d(\gamma(\theta) + \gamma_0)}{4}, & \frac{3\pi}{2} \leq \theta < \frac{3\pi}{2} + \Theta \\ -\frac{\mu k_n \varepsilon d}{k_t}, & \frac{3\pi}{2} + \Theta \leq \theta < 2\pi, \end{cases} \quad (78)$$

$$u_{13}^{(t)} = u_{12}^{(t)}, \quad (79)$$

$$u_{23}^{(t)} = 0, \quad (80)$$

where  $\Theta$  satisfies

$$-\frac{\mu k_n \varepsilon d}{k_t} - 3d \frac{\gamma(\frac{\pi}{2} + \Theta) - \gamma_0}{4} = \frac{\mu k_n \varepsilon d}{k_t}. \quad (81)$$

This equation provides  $\Theta = \cos^{-1}(1 - 2\gamma_c/\gamma_0)$ . Substituting these equations into  $f_{ij}^{(t)} = -k_t u_{ij}^{(t)}$  yields

$$f_{12}^{(t)} = \begin{cases} -\mu k_n \varepsilon d, & 0 \leq \theta(\theta) < \frac{\pi}{2} \\ -\mu k_n \varepsilon d - \frac{3k_t d(\gamma(\theta) - \gamma_0)}{4}, & \frac{\pi}{2} \leq \theta < \frac{\pi}{2} + \Theta \\ \mu k_n \varepsilon d, & \frac{\pi}{2} + \Theta \leq \theta < \frac{3\pi}{2} \\ \mu k_n \varepsilon d - \frac{3k_t d(\gamma(\theta) + \gamma_0)}{4}, & \frac{3\pi}{2} \leq \theta < \frac{3\pi}{2} + \Theta \\ -\mu k_n \varepsilon d, & \frac{3\pi}{2} + \Theta \leq \theta < 2\pi, \end{cases} \quad (82)$$

$$f_{13}^{(t)} = f_{12}^{(t)}, \quad (83)$$

$$f_{23}^{(t)} = 0. \quad (84)$$

The normal component of  $\sigma$  in eqn. (9) is given by

$$\sigma^{(n)} = \sigma_{12}^{(n)} + \sigma_{13}^{(n)} \quad (85)$$

with

$$\sigma_{12}^{(n)} = -\frac{1}{A} \frac{x_{12}y_{12}}{r_{12}} f_{12}^{(n)} \quad (86)$$

$$\sigma_{13}^{(n)} = -\frac{1}{A} \frac{x_{13}y_{13}}{r_{13}} f_{12}^{(n)}. \quad (87)$$

Substituting eqns. (56) and (57) with eqns. (62) and (63) into eqns. (86) and (87) and using eqn. (85), we obtain  $\sigma^{(n)}$  as eqn. (14).

The tangential component of  $\sigma$  in eqn. (10) is given by

$$\sigma^{(t)} = \sigma_{12}^{(t)} + \sigma_{13}^{(t)} \quad (88)$$

with

$$\sigma_{(12)}^{(t)} = -\frac{1}{2A} \frac{x_{12}^2 - y_{12}^2}{r_{12}} f_{12}^{(t)} \quad (89)$$

$$\sigma_{(13)}^{(t)} = -\frac{1}{2A} \frac{x_{13}^2 - y_{13}^2}{r_{13}} f_{12}^{(t)}. \quad (90)$$

Substituting eqns. (56) and (57) with eqn. (76) into eqns. (88), (89), and (90), we obtain  $\sigma^{(t)}$  as eqn. (15) for  $\gamma_0 < \gamma_c$ . Using eqns. (82) and (83) instead of eqn. (76), we obtain  $\sigma^{(t)}$  as eqn. (17) for  $\gamma_0 \geq \gamma_c$ .

The pressure, i.e.,  $P$ , in eqn. (11) is defined as

$$P = P_{12} + P_{13} + P_{23} \quad (91)$$

with

$$P_{ij} = \frac{1}{2A} r_{ij} f_{ij}^{(n)}. \quad (92)$$

Substituting eqns. (56)-(58) with eqns. (62)-(64) into eqns. (91) and (92) with  $\gamma = 0$ , we obtain  $P_0(\gamma_0, \mu)$  as eqn. (21).

## Appendix D: Relation between shear modulus and stress–strain curve

In this section, we relate the shape of the stress–strain curve to the complex shear modulus. The shear stress  $\sigma(\theta)$  is expanded using the Fourier series as

$$\sigma(\theta) = \gamma_0 \sum_{n=1}^{\infty} G'_n \sin(n\theta) + \gamma_0 \sum_{n=1}^{\infty} G''_n \cos(n\theta), \quad (93)$$

where  $G'_n$  and  $G''_n$  with  $n > 1$  denote the higher harmonics,  $G' = G'_1$ , and  $G'' = G''_1$ . By neglecting  $G'_n$  and  $G''_n$  for  $n > 1$ ,

$$G' \simeq \frac{\sigma(\theta = \pi/2)}{\gamma_0} = \frac{\sigma}{\gamma_0} \Big|_{\gamma/\gamma_0=1} = \tilde{\sigma}_{\max}, \quad (94)$$

which is the maximum value of the scaled stress–strain curve illustrated in Fig. 3(b). This expression and the scaled stress–strain curve in Fig. 3(b) explain the decrease of  $G'$  defined by eqn. (18).

The area  $S$  of the curve for  $\sigma(\theta)/\gamma_0$  against  $\gamma(\theta)/\gamma_0$  is given by

$$S = \int_0^{2\pi} d\theta \frac{1}{\gamma_0} \frac{d\gamma(\theta)}{d\theta} \frac{\sigma(\theta)}{\gamma_0}. \quad (95)$$

Substituting eqn. (4) into eqn. (95) with eqn. (12), we obtain

$$S = \int_0^{2\pi} d\theta \sigma(\theta) \cos \theta / \gamma_0 = \pi G'', \quad (96)$$

which results in  $G'' = S/\pi$ . As  $\gamma_0$  increases, the area  $S$  of the scaled stress–strain curve in Fig. 3(b) increases first and decreases later, which explains the  $\gamma_0$ -dependence of  $G''$  provided by eqn. (19).

## Appendix E: Details of Disordered MBS

In this section, we present the details of the disordered MBS. This model is an extension of the monodisperse model used in Appendix A, including the dispersion of the particles and disordered initial configuration.

The system is bidisperse and includes an equal number of particles with diameters  $d$  and  $d/1.4$ . To simulate the disordered MBS, we randomly place the particles in a rectangular box with an initial packing fraction of  $\phi_1 = 0.75$ . The system is slowly compressed until the packing fraction reaches  $\phi^{24}$ . In each compression step, the packing fraction is increased by  $\Delta\phi = 1.0 \times 10^{-4}$  with an affine transformation. Thereafter, the particles are relaxed to a mechanical equilibrium state with the kinetic temperature  $T_K = \sum_i p_i^2 / (mN) < T_{\text{th}}$ . Here, we choose  $T_{\text{th}} = 1.0 \times 10^{-8} k_n d^2$ . After compression, the oscillatory shear strain given by eqn. (4) is applied for  $N_c$  cycles. In the last cycle, we measure  $G'$  and  $G''$  using eqns. (12) and (13) with eqns. (8)–(10). The pressure,  $P_0(\gamma_0, \mu)$  is obtained using eqn. (11) after the last cycle. We use  $\phi = 0.87$ ,  $N = 1000$ ,  $N_c = 20$ ,  $L_y/L_x = 1$ ,  $k_t = 0.2k_n$ , and  $\eta_n = \eta_t = k_n \sqrt{m/k_n}$ .

Figure 12 shows the storage modulus  $G'$  against  $\gamma_0$  in the disordered MBS for various values of  $\mu$ . The storage modulus  $G'$  is almost independent of  $\gamma_0$  for a small  $\gamma_0$  and decreases as  $\gamma_0$  increases. The endpoint of the first plateau increases with  $\mu$  except for  $\mu = 0$ . A second plateau of  $G'$  exists for  $\mu = 10^{-4}$  and  $10^{-5}$ . The behavior of  $G'$  for relatively small  $\gamma_0$  is similar to that

of crystalline solids as depicted in Fig. 4. On the other hand, the decrease of  $G'$  for larger  $\gamma_0$  cannot be captured by the analytical results of the TBS. Note that  $G'$  for  $\mu = 0.1$  in the limit  $\gamma_0 \rightarrow 0$  is different from that for  $\mu \leq 0.01$ , which results from the  $\mu$  dependence of the jamming point  $\phi_j^9$ .

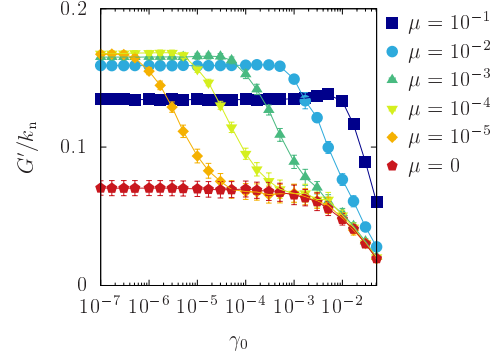


**Fig. 12** Storage modulus  $G'$  in the disordered MBS against  $\gamma_0$  with  $\phi = 0.870$  for various values of  $\mu$ .

Figure 13 shows the loss modulus  $G''$  in the disordered MBS against  $\gamma_0$  for various values of  $\mu$ . For sufficiently small  $\gamma_0$ ,  $G''$  is zero, while  $G''$  becomes non-zero as  $\gamma_0$  increases. The loss modulus  $G''$  starts to increase for smaller  $\gamma_0$  as  $\mu$  decreases. Similar to the case of  $G'$ , TBS captures only the behavior of relatively small  $\gamma_0$  (see Figs. 5 and 13).

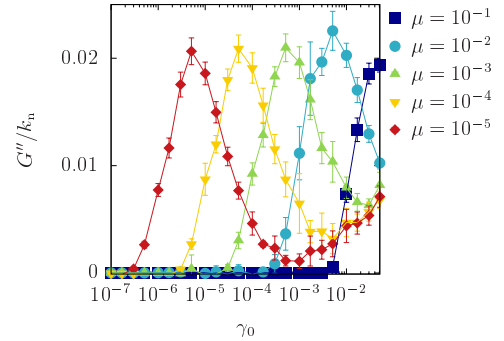


**Fig. 13** Loss modulus  $G''$  in the disordered MBS against  $\gamma_0$  with  $\phi = 0.870$  for various values of  $\mu$ .

## Appendix F: Numerical shear modulus for TBS

In this section, we show the behaviors of  $G'$  and  $G''$  in the TBS without the assumption used to obtain the analytical solution. Here, we numerically obtain  $G'$  and  $G''$  under quasistatic oscillation using eqns. (12) and (13) based on the left Riemann sum, where the integration of  $\Psi(\theta)$ , i.e.,

$$\int_0^{2\pi} d\theta \Psi(\theta), \quad (97)$$

is approximated as

$$\int_0^{2\pi} d\theta \Psi(\theta) \simeq \sum_{n=1}^M \Psi(\theta_n) \Delta\theta \quad (98)$$

with  $\Delta\theta = 2\pi/M$  and  $\theta_n = (n-1)\Delta\theta$ . We use  $\varepsilon = 0.001$  and  $\Delta\theta = 5.0 \times 10^{-5}$  in our simulation.

As shown in Fig. 14, we plot the storage modulus  $G'$  numerically obtained from the TBS against  $\gamma_0$  with  $k_t/k_n = 1.0$  for various values of  $\mu$  as points. Moreover, we plot the analytical results derived from eqn. (18) as thin solid lines. The numerical results agree with the analytical results for  $\gamma_0 < 0.003$  and reproduce the second plateau of the MBS shown in Fig. 4.

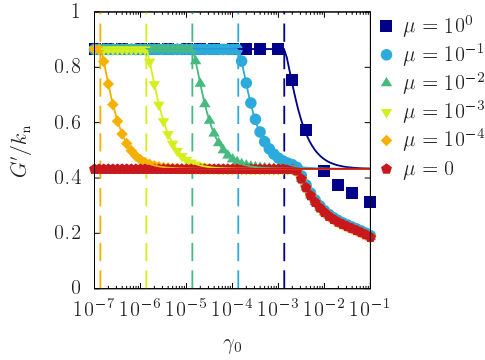


**Fig. 14** Storage modulus  $G'$  against  $\gamma_0$  with  $k_t/k_n = 1.0$  and  $\varepsilon = 0.001$  for various values of  $\mu$ . The points represent the numerical results of the TBS, while the thin solid lines represent the analytical result given by eqn. (18). The vertical dashed lines represent the critical amplitude  $\gamma_c(\mu)$  given by eqn. (16) for  $\mu = 10^{-4}, 10^{-3}, 10^{-2}, 10^{-1}, 10^0$  from left to right.

Figure 15 shows the loss modulus  $G''$  numerically obtained from the TBS against  $\gamma_0$  with  $k_t/k_n = 1.0$  for various values of  $\mu$  as points. We also plot the analytical results given by eqn. (19) as thin solid lines. The numerical results agree with the analytical results for  $\gamma_0 < 0.003$ .

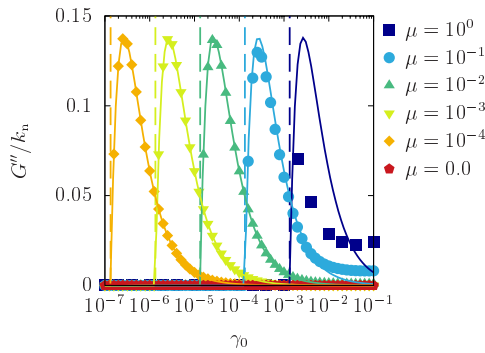


**Fig. 15** Loss modulus  $G''$  against  $\gamma_0$  with  $k_t/k_n = 1.0$  and  $\varepsilon = 0.001$  for various values of  $\mu$ . The points represent the numerical results of the TBS, while the thin solid lines represent the analytical results obtained from eqn. (19). The vertical dashed lines represent the critical amplitude  $\gamma_c(\mu)$  obtained from eqn. (16) for  $\mu = 10^{-4}, 10^{-3}, 10^{-2}, 10^{-1}, 10^0$  from left to right.

## Acknowledgements

The authors thank K. Saitoh, D. Ishima, and S. Takada for fruitful discussions. This study was supported by JSPS KAKENHI under Grant Nos. JP19K03670 and JP21H01006.

## Notes and references

- 1 M. van Hecke, *J. Phys.: Condens. Matter*, 2010, **22**, 033101.
- 2 R. P. Behringer and B. Chakraborty, *Rep. Prog. Phys.*, 2019, **82**, 012601.
- 3 C. Maloney and A. Lemaître, *Phys. Rev. E*, 2004, **93**, 195501.
- 4 C. E. Maloney and A. Lemaître, *Phys. Rev. E*, 2006, **74**, 016118.
- 5 D. Ishima, K. Saitoh, M. Otsuki and H. Hayakawa, 2022, arXiv:2207.06632.
- 6 C. S. O'Hern, S. A. Langer, A. J. Liu and S. R. Nagel, *Phys. Rev. Lett.*, 2002, **88**, 075507.
- 7 M. Wyart, *Ann. Phys.*, 2005, **30**, 1.
- 8 B. P. Tighe, *Phys. Rev. Lett.*, 2011, **107**, 158303.
- 9 M. Otsuki and H. Hayakawa, *Phys. Rev. E*, 2017, **95**, 062902.
- 10 C. Coulais, A. Seguin and O. Dauchot, *Phys. Rev. Lett.*, 2014, **113**, 198001.
- 11 M. Otsuki and H. Hayakawa, *Phys. Rev. E*, 2014, **90**, 042202.
- 12 K. H. Nagamanasa, S. Gokhale, A. K. Sood and R. Ganapathy, *Phys. Rev. E*, 2014, **89**, 062308.
- 13 E. D. Knowlton, D. J. Pine and L. Cipelletti, *Soft Matter*, 2014, **10**, 6931–6940.
- 14 T. Kawasaki and L. Berthier, *Phys. Rev. E*, 2016, **94**, 022615.
- 15 P. Leishangthem, A. D. S. Parmar and S. Sastry, *Nat. Commun.*, 2017, **8**, 14653.
- 16 A. H. Clark, J. D. Thompson, M. D. Shattuck, N. T. Ouellette and C. S. O'Hern, *Phys. Rev. E*, 2018, **97**, 062901.
- 17 J. Boschan, S. Luding and B. P. Tighe, *Granular Matter*, 2019, **21**, 58.
- 18 J. Boschan, D. Vågberg, E. Somfai and B. P. Tighe, *Soft Matter*, 2016, **12**, 5450–5460.
- 19 D. Nakayama, H. Yoshino and F. Zamponi, *J. Stat. Mech.*, 2016, **2016**, 104001.
- 20 T. Kawasaki and K. Miyazaki, 2020, arXiv:2003.10716.
- 21 K. Hyun, M. Wilhelm, C. O. Klein, K. S. Cho, J. G. Nam, K. H. Ahn, S. J. Lee, R. H. Ewoldt and G. H. McKinley, *Prog. Polym. Sci.*, 2011, **36**, 1697.
- 22 S. Dagois-Bohy, E. Somfai, B. P. Tighe and M. van Hecke, *Soft Matter*, 2017, **13**, 9036–9045.
- 23 D. Ishima and H. Hayakawa, *Phys. Rev. E*, 2020, **101**, 042902.
- 24 M. Otsuki and H. Hayakawa, *Eur. Phys. J. E*, 2021, **44**, 70.
- 25 M. Otsuki and H. Hayakawa, *Phys. Rev. Lett.*, 2022, **128**, 208002.
- 26 N. Goldenfeld, *Lectures on Phase Transitions and the Renormalization Group*, CRC Press, 1992.
- 27 J. E. Lennard-Jones and A. F. Devonshire, *Proc. R. Soc. A: Math. Phys. Eng. Sci.*, 1937, **163**, 53–70.
- 28 J. E. Lennard-Jones and A. F. Devonshire, *Proc. R. Soc. A: Math. Phys. Eng. Sci.*, 1938, **165**, 1–11.
- 29 F. Yonezawa and K. Morigaki, *Prog. Theor. Phys. Suppl.*, 1973, **53**, 1–76.
- 30 S. Feng, M. F. Thorpe and E. Garboczi, *Phys. Rev. B*, 1985, **31**, 276–280.
- 31 A. Awazu, *Phys. Rev. E*, 2001, **63**, 032102.

- 32 P. A. Cundall and O. D. L. Strack, Géotechnique, 1979, **29**, 47–65.
- 33 M. Doi and S. F. Edwards, The theory of polymer dynamics,

- Oxford University Press, 1986.
- 34 D. J. Evans and G. Morriss, Statistical Mechanics of Nonequilibrium Liquids, Cambridge University Press, 2008.